Vertical profiles of black carbon and nanoparticles pollutants measured by a tethered balloon in Longyerbyen (Svalbard islands)

David Cappelletti[a,i*] Chiara Petroselli[a], David Mateos[b], Marcos Herreras[b], Luca Ferrero[c], Niccolò Losi[c], Asta Gregorič[d], Claudia Frangipani[a,i], Gianandrea La Porta[a], Michael Lonardi[e], D.G. Chernov[f], Alena Dekhtyareva[g,h]

[a]TRACES Lab, Department of Chemistry, Biology and Biotechnology, University of Perugia, Perugia, Italy;

[b]Atmospheric Optics group, Department of Theoretical Physics, Atomic and Optics, University of Valladolid, Valladolid, Spain; ORCID ID: 0000-0001-5540-4721

[c]GEMMAcenter, Department of Environment and Earth Sciences, The University of Milano-Bicocca, Milan, Italy;

[d]Department of Research & Development, Aerosol d.o.o., Ljubljana, Slovenia

[e]Leipzig Institute for Meteorology, Lipzig, Germany

[f]Laboratory of Aerosol Optics, Division of the Radiation Components of the Climate, V.E. Zuev Institute of Atmospheric Optics of Siberian Branch of the Russian Academy of Science (IAO SB RAS), Tomsk, Russia

[g]Department of Engineering and Safety, Faculty of Engineering and Technology, UiT The Arctic University of Norway, Tromsø, Norway, ORCID iD;

[h]Geophysical Institute, University of Bergen, and Bjerknes Centre for Climate Research, Bergen, Norway, ORCID iD 0000-0003-4162-7427,

[i]ISP-CNR, Istituto di SciensePolari, del Consiglio NazionaledelleRicerche, Bologna, Italy

*corresponding author: david.cappelletti@unipg.it

Abstract

Airborne meteorological and aerosol measurements have been performed in Longyearbyen (Svalbard islands) in the Summer of 2018, coupling an instrumental aerosol payload with a meteorological radiosonde deployed on a tethered balloon. More than 70 vertical profiles of aerosol and meteorological properties have been recorded up to a maximum altitude of 1.2 km. As a main result, the present work provides a homogeneous gridded dataset of vertical profiles of equivalent black carbon (*eBC*) and nanoparticles (*NP*) concentrations and associated meteorological data (temperature, T, relative humidity, RH, pressure, P) to be employed for future modelling studies of Arctic pollution. Mean values (± SD) of *eBC* and *NP* below 500 m were 110±10 ng m^{-3} and 1400±400 particles cm^{-3}, respectively. Mean values above 500 m were 150±30 ng m^{-3} and 1000±350 particles cm^{-3}, respectively. Group medians of maximum *eBC* and *NP* concentrations in vertical profiles with temperature inversions were significantly higher than for those without inversion. The dataset has been complemented by continuous ground measurements of *eBC* with an average value of 208±130 ng m^{-3} (median value 110±70 ng m^{-3}) for the entire campaign; the ground-based background (absence of local emission) *eBC* value was below 100 ng m^{-3} while maximum values were in the 1000-2000 ng m^{-3} range. Median *eBC* concentration measured at ground for two hours before the tethered balloon launch was higher when temperature inversion was observed. The ground-based measurements, coupled with aerosol optical depth measurements, allowed for a preliminary discussion of two case studies related to high pollutants concentration events.

Keywords: aerosol vertical profiles, black carbon, nanoparticles, Arctic pollution

1. Introduction

Atmospheric pollution in the Arctic region is a topic of recent and great interest (Law and Stohl, 2007) as the Arctic is subject to an amplification of the global warming, with observed temperature increasing almost twice as fast with respect to the global average (Goosse et al., 2018; Serreze and Barry, 2011). Typically, various contaminants are transported towards high latitudes, travelling over long distances in the atmosphere (Barrie et al., 1992). On the other hand, the recent anthropization of many Arctic regions poses the question of emerging local, anthropogenic sources of pollutants (Law et al., 2017; Schmale et al., 2018). These emission sources, that include coal and biomass combustion, oil and gas flaring, marine and terrestrial transportation (Roiger et al., 2015), may generate secondary pollutants such as ozone and nitrogen oxides, and hydrocarbons, including volatile organic compounds, carbon monoxide and methane, or aerosols such as black carbon or sulphate aerosols, typically in the nanoparticle-size range. Locally emitted pollutants may be dispersed in the atmosphere with different efficiencies; therefore, the knowledge of their vertical distribution is of great relevance to assess the local impacts on the local population and more generally on the Arctic region. Among the whole ensemble of atmospheric pollutants the aerosol is very important due to its role of short-lived climate forcer that can produce different climatic effects and local feedbacks depending on its vertical location (Ferrero et al., 2014; Goosse et al., 2018; Serreze and Barry, 2011; Su et al., 2020).

Understanding the vertical structure of aerosol pollutants in the Arctic atmosphere is very complex and challenging. The reasons are related to the very low aerosol concentrations, the effect of long-range advections, and the effect of local winds and orography. The combined result of these factors may lead to layered pollution, which should be investigated accounting for the influence of different sources at different altitudes (Thomas et al., 2019). Long-range transported aerosols tend to show higher concentrations in the free troposphere, while emerging anthropogenic sources within the Arctic have been causing intense summer plumes confined in the atmospheric boundary layer and in proximity of the emission hotspot (Mayfield and Fochesatto, 2013).

Experimental studies of *eBC* and *NP* vertical distribution in the Arctic atmosphere are scarce and with inhomogeneous spatial and temporal coverage, if compared with the number of available data collected at ground level (Samset et al., 2014). Remote sensing observations, both from satellites and ground-based instruments, indicate that the highest aerosol concentration in all sectors of the High Arctic and throughout the whole year is observed in the lowest kilometre of the atmosphere (Devasthale and Thomas, 2011; Shibata et al., 2018). The efficiency of long-range transport of anthropogenic pollutants to Svalbard depends on the position of the Arctic front. In winter and spring, the front shifts southwards and allows for more frequent transport of air masses from mid-latitudes to the Arctic with a phenomenon called Arctic haze (Quinn et al. 2007), while, in summer, the front shifts northwards, and the relative importance of local anthropogenic emission sources and their contribution to the total pollution load may increase. Thus, the winter-spring aerosol concentration changes as a function of altitude, indicating the influence of different sources and transport at different altitudes (Shibata et al., 2018) (Doherty et al., 2013) (Creamean et al., 2021). Beside the remote sensing observations that are fundamental tools to monitor the vertical variability of atmospheric aerosol on large spatial and long temporal scale, in-situ airborne aerosol observations can provide insights on aerosol physics and chemistry. Validation of remote sensing (lidar) data with in-situ (tethered balloons) experiments has been recently proposed (Ferrero et al., 2019). During the Arctic haze period, black carbon concentration tends to increase with altitude since the first kilometre from the ground (Ferrero et al., 2016; Markowicz et al., 2017) showing a gradual increase till mid altitudes (~1 km). In general, lower altitudes were influenced mainly by local Arctic sources, while mid- and upper levels were indicate transport from eastern Europe, northern and central Asia (Schulz et al., 2019).

In order to improve the knowledge on aerosol vertical profiles in the Arctic area, the present paper presents a set of vertical aerosol profiles recorded by tethered balloon experiments in Longyearbyen, the major urban settlement in Svalbard Islands, European Arctic. The main goal of the work is to provide the scientific community with a homogenized dataset of vertical aerosol profiles for further investigations in the coupled modelling-measurements studies. The atmospheric pollutants investigated in this study are equivalent black carbon (*eBC*) and nanoparticles (*NP*). The experimental methodology adopted in the present work is presented in Section 2. Results and their discussion are presented in Section 3. This section presents a detailed analysis of the factors shaping the aerosol vertical structure. In particular, average concentration ranges and dependence on temperature inversions are presented in Sec. 3.3. Moreover, Section 3.4 presents a comparison between *eBC* and *NP* profiles which highlights the relative role of local source and long-range transport. A focus on long-range episodes is illustrated in Sec. 3.5. Finally, the homogenized vertical profile dataset is presented in Sec. 3.6. Conclusions follows in Sec. 4.

2. Experimental methodology

2.1 Tethered balloon launching site

Tethered balloon launches were performed during summer 2018, between July and August, in Longyearbyen (LYB), in the centre of Spitsbergen (Figure 1a), specifically from the CO_2 laboratory of the University Centre in Svalbard (UNIS) located in the Adventdalen valley, approximately 5 km to the south-east of Longyearbyen (Figure 1b). LYB is the world's northernmost settlement with more than 2000 inhabitants, however, the high touristic fluxes that showed a notable increase in the last decades, often determine a substantial increase of this number. The specific pollution emission sources connected to touristic activities add to those related to coal mining activities, coal power generation, naval and airplane traffic, making LYB an interesting case study for Arctic air pollution.

The two biggest settlements in Svalbard, namely Longyearbyen and Barentsburg, are located on two branches of the wide Isfjorden fjord (Figure 1a), called Adventfjorden (eastern branch) and Grønfjorden (southern branch) respectively. Both cities are subjected to heavy naval traffic which represents one of the most relevant pollution sources in the area. In fact, until 2022 the Isfjorden was not part of the area where a strict regulation on ship's fuel (no use of heavy fuel oil) was applied and it was thus still allowed to use oil with sulphur content up to 3.5% in 2018. Moreover, transport ships to and from Longyearbyen and Barentsburg will not be subjected to the new regulations, that will be enforced starting from January 2022, which will prohibit the usage of heavy oil in the whole Svalbard territorial waters.

The choice of the launching site was based on two main reasons. The first one is that local pollution from ships and the power plant emissions may reach the UNIS CO_2 station only if the north-westerly wind is prevailing; the second one is related to airport safety, in fact the site is far enough from the airport so that it does not interfere with the aircraft traffic in the area. Indeed, the cooperation with the Svalbard Airport of LYB allowed to record all the vertical profile measurements in the hours when no planes or helicopters were arriving or departing from LYB.

The tethered balloon used to perform vertical profiles (filled with 3.25 m^3 of helium) was operated in the hours when ground-based wind speed was below 10 m/s since stronger wind could potentially damage the equipment. In the days when the launch was cancelled due to high wind speed, the wind was in the direction from the Adventdalen valley, therefore, there was no influence of local air pollution from the town on concentrations near the UNIS CO_2 lab.

According to all the aforementioned meteorological and operational restrictions, we managed to obtain 78 (39 up and 39 down) vertical meteorological profiles, recorded in 52 days of ground-based measurements. 95% of the launches were performed between 12:00 and 18:00 UTC, and only 5% were made from 18:00 to 00:00.

2.2 The aerosol payload

The instrumental payload consisted in a Vaisala meteorological sensors recording *T*, *P* and *RH* data, a micro-aethalometer AE51 for *eBC* data (Ferrero et al., 2011) and a portable particle counter (MiniDISC, Matter aerosol) for *NP* data (Ferrero et al., 2016).

The AE51 microaethalometer (Aethlabs, USA) is a light portable device that records the light attenuation due to the aerosol loading on a glass-fiber filter at the wavelength of 880 nm. The equivalent black carbon mass concentration (*eBC*) is derived from standard formulas (HANSEN et al., 1984) using a mass attenuation cross-section coefficient of 12.5 m^2 g^{-1}, calibrated by the manufacturer. The AE51 was operated with a flux of 200 mL min^{-1} and a time interval of 30 seconds. Filters have been changed regularly to keep the filter loading as low as possible. Therefore, data have not been compensated for the loading effect.

The MiniDISC is a miniature diffusion size classifier, a small and portable instrument (Fierz et al., 2011). This device has a d50 cut-off at 14 nm, therefore, it underestimates particle number concentrations for particles smaller than 20 nm while, above this threshold, acts as a total particle counter. The instrument was operated at 1 second time resolution and the data were post-processed at 10 seconds with the Java routine supplied by the manufacturer.

Both the MiniDISC and AE51 have not been deployed on the balloon when the air humidity was too high (relative humidity above 90% was used as a threshold). Moreover, the MiniDISC has been employed for a shorter period of time (6 Jul-11Aug) than the AE51 (3 Jul-15 Aug). In total, 74 equivalent black carbon (eBC) and 52 nanoparticle number (NP) concentration profiles were obtained.

2.3 Vertical profile data post-processing

In order to reduce the noise of concentration data obtained using high time resolutions, post-processing algorithms were used. This procedure is particularly important for the *eBC* data, which show a high point-to-point variability while *NP* measurements are more stable. The following procedure has been implemented:

1) The rate of pressure and temperature change with time dP/dt and dT/dt have been calculated for ascending and descending profiles separately.

2) The calculated rates have been checked for normality of distribution using Kolmogorov-Smirnov test in the Matlab software.

3) Since the data are not normally distributed, a robust measure to detect outliers has been chosen. The outliers in the dP/dt and dT/dt data were identified as the ones showing values which were more than three scaled median absolute deviation (MAD) from the median values (Rousseeuw and Hubert, 2011).

4) Pressure values for these outlier points are changed to the linearly interpolated value between closest non-outlier pressure points. As the sampling rate is irregular, the interpolation is done considering local time interval between two nearest non-outlier points. This method removes only extreme outliers; it does not smooth the data and the processing result is still close to the original values.

5) The height has been calculated from pressure using a hypsometric equation (Wallace and Hobbs, 2006), which is common to use for radiosonde profiles.

6) To compare *eBC* (or *NP*) profiles with the meteorological values, the height, temperature

and wind speed have been averaged for 30 sec time periods according to the timing at AE51 (or *NP*) sensor.

7) *eBC* data smoothing has been performed using a 1-2-1 smoothing filter as suggested by (Wang and Wang, 2014); Accordingly to this method, the smoothed value at a given altitude is the weighted average of the values at the previous altitude (with a 25% weighting factor), at the altitude of interest (with a 50 % weighting t factor), and at a the following with a 25% weighting factor. Even after the smoothing, the AE51 provided few negative values for *eBC*. The proportion of negative values of *eBC* was 11.2 %, considering the raw data at 30 s acquisition time. After the 50 m averages used to grid the dataset (see below) the proportion of negative values reduced to 7.1%. These values are in agreement with other experiments carried out with the AE51 (Miyakawa et al., 2020).

Both instruments were previously tested and compared with ground-based bench instruments in Ny-Ålesund(Ferrero et al., 2016; Moroni et al., 2015), which provided an assessment of their accuracy and detection limits.

2.4 Complementary ground-based aerosol measurements and inter-comparison of eBC data

The vertical profiles dataset was complemented with several other measurements within a larger experimental campaign. Of particular relevance for the present paper, a seven channels Aethalometer model AE33 (Magee Scientific) was placed in the office on the third floor at UNIS building in LYB, where the inlet of the sampling hose was fixed outside from the window. The data have been accumulated continuously at 1 min time resolution and 5 l/min flow rate for the whole field campaign. Meteorological data have also been recorded along the campaign.

An in-situ intercomparison of the AE51 and the AE33 at the UNIS site was carried out eight times throughout the campaign with an average calibration period of two hours each time. The temperature, humidity and wind speed ranges during the calibrations were 4.4-14.4℃, 60-100%, 0-7.6m·s^{-1}, respectively. AE33 data with 1-min time resolution were compared with 1-min averaged data from AE51. The worst and the best correlation between the two instruments were obtained on 21/07/2018 and 01/08/2018 when the mean concentration of *eBC* measured by AE33 was the lowest (191 ng·m^{-3}) and the highest (1051 ng· m^{-3}), respectively. The correlation between the *eBC* values of the two instruments was calculated for the four groups of data (quartiles). Results of intercomparison show a better agreement in the higher concentrations range.

The same procedure was done for quartiles of air temperature, relative humidity and wind speed to check if these values influenced the correlation, but no significant difference in correlation coefficients has been found for different groups within the range of meteorological parameters during calibration. Details of the inter-comparison are reported in the Supplementary Material.

Since the concentrations of *eBC* measured during soundings in Adventdalen were very low, often within the 1st quartile of AE33 data, high uncertainty in absolute values of *eBC* data measured by AE51 has to be considered. However, since 50m-average values were applied to study profiles' statistics, this averaging eliminated some of the noise.

Columnar AOD data from Longyearbyen, Ny-Ålesund, and Barentsburg have also been investigated. The two former sites belong to AERONET (Longyearbyen and Ny_Alesund_AWI sites) and data from version 3 – level 2.0 are presented here. The data fromBarentsburg were obtained using SP-9 sun photometer that measured solar irradiance between 300 and 2200 nm. The instrument is equipped with GPS, tracker and cloud screening.

3 Results and discussion

3.1 Weather conditions in the study area

Weather conditions in the investigated area are determined by the combination of synoptic circulation and local topography. Winds aloft are typically south-westerly or north-easterly (Hanssen-Bauer and Førland, 2001). Several low pressure systems were recorded during the investigated period, approaching from the south-west and bringing warmer air. The orography of the area, characterized by 500 m high plateaus separated by valleys, controls the flows at lower altitudes (Mayer et al., 2012), with wind channelling occurring in the valleys. The study period covers the transition between the summer solstice and the end of the polar day (3 July-15 August, 2021). The surface energy budget is impacted by large solar irradiances and low albedo.

Local conditions in the Adventdalen valley were derived using hourly data from the local 10 m weather mast. A weather station located at 464 m a.s.l. on the neighbouring plateau Gruvefjellet was used to gain representative data for the upper parts of the balloon's vertical profiles. The topography surrounding the balloon site typically induce wind channelling along the Adventdalen valley (~135° and ~315°), decoupling the lowermost 400-500 m of the Atmospheric Boundary Layer (ABL) from the large-scale circulation. A diurnal cycle in winds and temperature in Adventdalen gradually gained importance in August. The wind aloft the plateau was generally southerly or easterly, following the synoptic circulation. The wind inside the valley was typically channelled from Adventfjord towards the station (Figure SM1a). An average wind speed of 3-4 m s^{-1} was measured at the mountain and the valley sites, with intensities never dropping below 1 m s^{-1} (Figure SM1b).

Three periods were particularly influenced by the synoptic activity: (L) 8-13 July, (L) 22-26 July and (H) 2-6 August. During these events, the passage of pressure systems was associated with increased wind speeds and constant wind directions inside and above the valley.

The surface temperature at the Old Auroral Station was 7 °C on average, with temperature increasing until early August, when the maximum hourly temperature of 12 °C was recorded (Figure SM1c). Temperature at the mountain site (Gruvefjellet) was generally lower due to the height difference. Humidity was systematically above 60% (Figure SM1d), with low-level clouds forming above the valley.

3.2 Construction of gridded vertical profiles

The post-processed vertical profiles of *eBC* and *NP* are reported in Figure 2.

Most of the profiles covered the first 750 m and only six launches reached the elevation of 1 km. In general, *eBC* profiles showed a larger variability both in magnitude and in vertical trend as compared to the *NP* profiles. The strong negative *eBC* signal in one of the profiles (below 250 m a.g.l.) was caused most probably by the intense wind (>6 m s^{-1}) blowing at ground during the preparation and first part of the measurements.

The gridded vertical profile datasets have been constructed by averaging the pre-processed data accumulated in 50 m vertical bins and assigned to the middle height of the vertical bin (for example: the first point was generated at 25 m above ground, including data from 0 to 50 m). Data points in each vertical bin ranged from two to ten. The gridded profiles are presented in Figure 3.

Temperature (T), relative humidity (RH), pressure (P) and wind speed (ws) were also gridded on the same 50 m vertical scale. This allowed to study the general phenomenology and to produce seasonally averaged profiles on a homogeneous vertical grid.

3.3 Vertical profiles: general phenomenology

The maximum height of Adventdalen profiles was less than 500 m for 33% of profiles, 59% of the profiles were between 500 and 1000 m, and 8% above 1000 m. According to the WRS-test, median profile wind speed and air temperature below 1000 m were significantly higher for the measurements with temperature inversions height $zTb<500$ m, than for those with inversion starting above 500 m (shown in bold in Table 1). The opposite relationship was observed for relative humidity in the two groups. Profiles without temperature inversions had the highest median wind speed and lowest median profile temperature (see Table 1).

Synoptic scale meteorological situations for the three groups, which are defined as: (a) without temperature inversions in Adventdalen, (b) with temperature inversions detected below 500 m height and (c) with inversions starting above 500 m, are shown in Figure SM2. Both (a) and (b) groups of days were characterized by a high-pressure system located to the south-east of Svalbard. However, the south-westerly wind with higher wind speed was prevailing during the (a) group of measurements, while in the (b) group, the wind speed was lower and air masses transported from the south were warmer, due to higher air temperatures recorded over Scandinavia. In the (c) group of days ($zTb>500$m), the north-westerly wind with low wind speed was bringing humid air from North Atlantic to Svalbard. Results of wind measurements for the same three groups from Longyearbyen (24 m a.s.l.), Adventdalen (15 m a.s.l.) and Gruvefjellet (464 m a.s.l.) are shown in Figure SM2 (d, e and f.) The mean wind speed observed in Adventdalen was almost the same for the three groups, however, according to the data from the Gruvefjellet station, the wind speed aloft was lower for the days with temperature inversions. The wind direction in Adventdalen was always north-westerly, along the valley axis, while in the days without temperature inversion, the wind direction observed at Gruvefjellet (Fig. SM2d) was similar to the large scale flow (Fig. SM2a). In most cases, north-westerly and westerly wind direction in Longyearbyen was favourable for transport of local pollutants towards Adventdalen valley, where *eBC* soundings were performed, except for a few days when south-westerly flow was observed in town, similarly to the measurements made at the Gruvefjellet station.

3.4 comparison of eBC and NP vertical profiles

The statistics of vertical *eBC* and *NP* concentration measurements for the three groups, is reported in Table 1. There is a positive statistically significant correlation between the height of maximum *eBC* concentrations and height of minimum wind speed in the profiles ($r=0.44$, $p<0.001$). Indeed, in 92% of all profiles, the height of maximum *eBC* concentration is lower than or equal to the height of minimum wind speed. On average, maximum *eBC* concentrations could be found around 230m below the height of minimum wind speed. The correlation between the height of maximum concentration and the height of the maximum temperature was not statistically significant.

Since the number of profiles with *zTb*>=500m is very small, the groups (b) and (c) have been combined into one group, with 31 *eBC* profiles ($n_{BC}=31$) and 16 *NP* profiles ($n_{part}=16$), and compared to group (a) when no temperature inversions were observed ($n_{BC}=43$, $n_{part}=32$). According to the WRS-test, there is no statistically significant difference between median concentrations of *eBC* for the two groups, while the median concentration of *NP* in the profiles with temperature inversion was significantly higher than in profiles where no inversions were observed ($p<0.001$). Group medians of maximum *eBC* and *NP* concentrations in profiles with temperature inversions were significantly higher than for those without inversion. Similarly, median *eBC* concentration measured in Longyearbyen for two hours before the sounding to the time of tethered balloon launch with *eBC* sensor in Adventdalen was higher when temperature inversion was observed ($p<0.001$).

Homogeneous profiles for both *eBC* and *NP* have been observed for 35.7% of the cases for the present summertime 2018 campaign in Longyearbyen, which is in good agreement with the 40% homogeneous profiles observed in the summertime 2012 in Ny Alesund (Ferrero et al., 2016). In 23% of the cases *eBC* showed an increasing concentration profile with increasing altitude while only for 4% of the cases the opposite trend was observed. High eBC and NP concentrations at ground level (<300 m), have been observed for 9% of the cases (see Supplementary Material, figure SM3), similarly to the summertime 2012 in Ny Alesund (Ferrero et al., 2016). In 14% of the cases, we observed high concentration of *NP* at ground level accompanied with low values of *eBC* (see figure SM4). These situations could be attributed to both local sources emitting non-carbonaceous particles and to new particles formation events (Beck et al., 2021).

Overall, the correlation between *eBC* and *NP* concentration for the 52 simultaneous vertical profiles was low (correlation coefficient ~0.20) even if the correlation was better in the first 250 m of the profile (correlation coefficient up to 0.40). On the other hand, for 20% of the cases *eBC* and *NP* profiles showed a high correlation coefficient (in the 0.6-0.9 range). These cases included the high aerosol concentration at ground case described above and some homogeneous profiles, always characterised by the presence of ships in the LYB harbour. Long-range transport of *eBC*, phenomenologically individuated as a high altitude layer, has been observed for the 4 % of the cases. One example will be illustrated in the next section.

3.5 An example of use of the gridded dataset: local sources versus long-range transport

The present dataset can be exploited to unveil the relative role of local and long-range sources of pollutants in the Longyearbyen area. Hereby, we discuss a selected case study to investigate the influence of local versus remote sources to the *eBC* levels in LYB. The *eBC* general trend is well described by the data from AE33 instruments running in LYB on 1 minute time resolution. A preliminary analysis of this dataset provided background *eBC* values for the summer season in LYB, which were typically lower than 100 ng m^{-3}. The analysis also highlighted the presence of sharp *eBC* peaks lasting from 1 to 10 minutes with *eBC* values in the 1000-2000 ng m^{-3} range, which can be ascribed to the local pollution sources. The overall mean value of *eBC* for the campaign was 208±130 ng m^{-3} while the median value was 110±70 ng m^{-3}. The trends of the daily median of the 1 minutes *eBC* values together with the 25 and 75 percentiles are reported in Figure 4. Even after averaging, the daily values are significantly higher than the background, with a high day-to-day variability. We investigated two case studies: the 1st August during which the highest *eBC* daily value of the campaign, 780 ng m^{-3}, was reached, and the 13th of August, with a daily average *eBC* of 286 ng m^{-3}.

The vertical profiles of eBC, temperature and wind speed, recorded with the tethered balloon system on the 1st of August at 15:00 UTC and on the 13 of August at 16:30 UTC are reported in Figure 5. Unfortunately, *NP* profiles were not measured in these days. The profiles on the 1st of August clearly indicate a stratification of *eBC* in the first 200 meters associated with a temperature inversion at approximately 300 m a.s.l. and low wind speed pointing at an apparent influence of local sources. By contrast, a significant layer of *eBC* , up to nearly 600 ng m^{-3}, was present on the 13th of August around 900-1000 meters and associated with a high wind speed layer. The median eBC concentrations measured in profile from soundings in Adventdalen on that day were higher than average (294 ng m^{-3}). There was no pronounced temperature inversion, probably due to the mixing of the boundary layer due to high wind speed. It is noteworthy that on the 13th August, the wind speed and temperature profiles (Figure 5) highlight the presence of three distinct atmospheric layers: one from ground to 300 m a.g.l., one between 300 and 800 m and the last one above 800 m. Thus, the higher *eBC* concentration layer can be considered separated from the bottom one ensuring the non-local origin of its source. According to backward trajectories analyses (HYSPLIT (Stein et al., 2015)) for the 13th of August, the air masses were arriving from the Northern sectors of Eurasia (see Supplementary Material), where the probable source of *eBC* is located.

This aerosol outbreak event extended to the whole Svalbard archipelago and was also identified in the columnar AOD data from Longyearbyen, Ny-Ålesund, and Barentsburg. Figure 6a shows the general trend of the Ångström Exponent 440/870 nm as a function of the AOD at 500 nm for the three sites during the campaign. Data from the August 13th are highlighted with more intense colours. High AOD values (at 500 nm) between 0.2 and 0.7 are reported in the three sites simultaneously. As recorded in the three sites, there is a sharp increase in AOD values resulting in a doubling of the AOD values in less than 4 hours. No particular variation of the Ångström Exponent is observed in the archipelago during the aerosol outbreak. Ångström Exponent values are around 1.5 with a slight decrease up to 1.4, which indicates the predominant presence of small particles in the atmospheric column associated to the investigated event.

Figure 6b shows the size distribution inversions for August 13th for Longyearbyen and Ny-Ålesund (AERONET sites). There is a large concentration of particles with radius below 0.4 µm, so that event is dominated by the fine mode particles. The transport becomes stronger with time and no significant differences are observed between Longyearbyen and Ny-Ålesund (112 km apart).

3.6 Averaged vertical profiles

The gridded dataset also allowed to calculate averaged vertical profiles of the measured properties which represent a description of the summertime Longyearbyen atmospheric column. Results are shown in Figures 7-8 for *eBC, NP, T, RH* and wind speed, respectively.

The tethered balloon averaged profiles reported in Figures 7-8 highlight the presence of marked aerosol stratification for nanoparticles close to the ground and a higher level of *eBC* at higher altitude (above 500 m). The *eBC* behaviour was in accordance with a higher wind speed around 500 m. The aforementioned results describe a situation previously observed in late spring over Ny-Ålesund, in which a plume of nanoparticle (probably of secondary origin) is present close to the ground.

In this respect, it has been recently demonstrated that the final vertical aerosol profiles can result from the synergy between the seasonal behaviour of aerosol and the local meteorology (Brock et al., 2011; L. Ferrero et al., 2016; Jacob et al., 2010). The importance of classifying average aerosol profiles in function of the season and meteorological situation is related to their feedback on climate (Creamean et al., 2021; Ferrero et al., 2016; Samset et al., 2014).

4. Conclusion

The objective of the present work is to generate a homogeneous gridded dataset of aerosol vertical profiles recorded in a summertime campaign in Longyearbyen (Svalbard Islands). The main aerosol properties, such as equivalent black carbon and total particle concentrations, have been measured with a tethered balloon system within the first kilometre of the troposphere above this anthropized Arctic settlement.

Temperature inversions, determined by warm air advections from Scandinavia to Svalbard, promote favourable conditions for the accumulation of local pollutants in the Arctic boundary layer. However, elevated aerosol concentrations may be observed in Longyearbyen even in the absence of the long-range transported pollution. In these days, colder air masses were brought by the large-scale westerly wind. The wind direction changed to north-westerly due to channelling along the Adventdalen valley, and locally polluted air was efficiently transported from the major local emission sources, the coal power plant and ships, to the valley.

The vertical structure of summer ABL in Adventdalen (Longyearbyen) was similar to that of Ny-Ålesund (Ferrero et al., 2016; Moroni et al., 2016), with higher median wind speed and lower air temperatures in the profiles without temperature inversions and higher air temperature and lower wind speed in the profiles with inversions at both sites. In the days with temperature inversions, higher *eBC* and total particle concentrations were observed in Adventdalen profiles and by ground-based measurements in Longyearbyen.

Acknowledgements

Dr. Kim Holmén is gratefully thanked for the invaluable advice on local pollution sources in Ny-Ålesund and Longyearbyen. Research technician Vitaly Dekhtyarev is acknowledged for support with electronic equipment and data processing during the field work in Longyearbyen in 2018. We thank UNIS for providing meteo data. We also acknowledge the AMIS project and the GEMMA center in the framework of the MIUR project "Dipartimenti di Eccellenza 2018-2022".

Funding

The Research Council of Norway financed the pilot study in Longyearbyen. The field work was a part of the project "Strengthening cooperation on air pollution research in Svalbard" received the support via Svalbard Strategic Grant (n. 283475).

CRediTauthor statement

DC: Conceptualization, Methodology,Writing, Reviewing and Editing. **CP, AD, ML**: Investigation,Data curation, Writing, Reviewing and Editing.**AD:**Original draft preparation. **DM, MH, LF, DGC, GL, CF, AG**: Data curation,Reviewing and Editing.

Data Availability

The data that support the findings of this study are openly available in Pangaea at http://doi.org/[doi], reference number [reference number].

References

Barrie, L.A., Gregor, D., Hargrave, B., Lake, R., Muir, D., Shearer, R., Tracey, B., Bidleman, T., 1992. Arctic contaminants: sources, occurrence and pathways. Sci. Total Environ. 122, 1–74. https://doi.org/10.1016/0048-9697(92)90245-N

Beck, L.J., Sarnela, N., Junninen, H., Hoppe, C.J.M., Garmash, O., Bianchi, F., Riva, M., Rose, C., Peräkylä, O., Wimmer, D., Kausiala, O., Jokinen, T., Ahonen, L., Mikkilä, J., Hakala, J., He, X.C., Kontkanen, J., Wolf, K.K.E., Cappelletti, D., Mazzola, M., Traversi, R., Petroselli, C., Viola, A.P., Vitale, V., Lange, R., Massling, A., Nøjgaard, J.K., Krejci, R., Karlsson, L., Zieger, P., Jang, S., Lee, K., Vakkari, V., Lampilahti, J., Thakur, R.C., Leino, K., Kangasluoma, J., Duplissy, E.M., Siivola, E., Marbouti, M., Tham, Y.J., Saiz-Lopez, A., Petäjä, T., Ehn, M., Worsnop, D.R., Skov, H., Kulmala, M., Kerminen, V.M., Sipilä, M., 2021. Differing Mechanisms of New Particle Formation at Two Arctic Sites. Geophys. Res. Lett. 48, 1–11. https://doi.org/10.1029/2020GL091334

Brock, C.A., Cozic, J., Bahreini, R., Froyd, K.D., Middlebrook, A.M., McComiskey, A., Brioude, J., Cooper, O.R., Stohl, A., Aikin, K.C., De Gouw, J.A., Fahey, D.W., Ferrare, R.A., Gao, R.S., Gore, W., Holloway, J.S., Hübler, G., Jefferson, A., Lack, D.A., Lance, S., Moore, R.H., Murphy, D.M., Nenes, A., Novelli, P.C., Nowak, J.B., Ogren, J.A., Peischl, J., Pierce, R.B., Pilewskie, P., Quinn, P.K., Ryerson, T.B., Schmidt, K.S., Schwarz, J.P., Sodemann, H., Spackman, J.R., Stark, H., Thomson, D.S., Thornberry, T., Veres, P., Watts, L.A., Warneke, C., Wollny, A.G., 2011. Characteristics, sources, and transport of aerosols measured in spring 2008 during the aerosol, radiation, and cloud processes affecting Arctic Climate (ARCPAC) Project. Atmos. Chem. Phys. 11, 2423–

2453. https://doi.org/10.5194/acp-11-2423-2011

Creamean, J.M., De Boer, G., Telg, H., Mei, F., Dexheimer, D., Shupe, M.D., Solomon, A., McComiskey, A., 2021. Assessing the vertical structure of Arctic aerosols using balloon-borne measurements. Atmos. Chem. Phys. 21, 1737–1757. https://doi.org/10.5194/acp-21-1737-2021

Devasthale, A., Thomas, M.A., 2011. A global survey of aerosol-liquid water cloud overlap based on four years of CALIPSO-CALIOP data. Atmos. Chem. Phys. 11, 1143–1154. https://doi.org/10.5194/acp-11-1143-2011

Doherty, S.J., Grenfell, T.C., Forsström, S., Hegg, D.L., Brandt, R.E., Warren, S.G., 2013. Observed vertical redistribution of black carbon and other insoluble light-absorbing particles in melting snow. J. Geophys. Res. Atmos. 118, 5553–5569. https://doi.org/10.1002/jgrd.50235

Ferrero, L., Cappelletti, D., Busetto, M., Mazzola, M., Lupi, A., Lanconelli, C., Becagli, S., Traversi, R., Caiazzo, L., Giardi, F., Moroni, B., Crocchianti, S., Fierz, M., Mocnik, G., Sangiorgi, G., Perrone, M., Maturilli, M., Vitale, V., Udisti, R., Bolzacchini, E., 2016. Vertical profiles of aerosol and black carbon in the Arctic: A seasonal phenomenology along 2 years (2011-2012) of field campaigns. Atmos. Chem. Phys. 16. https://doi.org/10.5194/acp-16-12601-2016

Ferrero, Luca, Cappelletti, D., Busetto, M., Mazzola, M., Lupi, A., Lanconelli, C., Becagli, S., Traversi, R., Caiazzo, L., Giardi, F., Moroni, B., Crocchianti, S., Fierz, M., Močnik, G., Sangiorgi, G., Perrone, M.G., Maturilli, M., Vitale, V., 2016. Vertical profiles of aerosol and black carbon in the Arctic : a seasonal phenomenology along 2 years (2011 – 2012) of field campaigns. Atmos. Chem. Phys. 16, 12601–12629. https://doi.org/10.5194/acp-16-12601-2016

Ferrero, L., Castelli, M., Ferrini, B.S., Moscatelli, M., Perrone, M.G., Sangiorgi, G., D'Angelo, L., Rovelli, G., Moroni, B., Scardazza, F., Mocnik, G., Bolzacchini, E., Petitta, M., Cappelletti, D., 2014. Impact of black carbon aerosol over Italian basin valleys: High-resolution measurements along vertical profiles, radiative forcing and heating rate. Atmos. Chem. Phys. 14. https://doi.org/10.5194/acp-14-9641-2014

Ferrero, L., Mocnik, G., Ferrini, B.S., Perrone, M.G., Sangiorgi, G., Bolzacchini, E., 2011. Vertical profiles of aerosol absorption coefficient from micro-Aethalometer data and Mie calculation over Milan. Sci. Total Environ. 409, 2824–2837. https://doi.org/10.1016/j.scitotenv.2011.04.022

Ferrero, L., Ritter, C., Cappelletti, D., Moroni, B., Močnik, G., Mazzola, M., Lupi, A., Becagli, S., Traversi, R., Cataldi, M., Neuber, R., Vitale, V., Bolzacchini, E., 2019. Aerosol optical properties in the Arctic: The role of aerosol chemistry and dust composition in a closure experiment between Lidar and tethered balloon vertical profiles. Sci. Total Environ. 686. https://doi.org/10.1016/j.scitotenv.2019.05.399

Fierz, M., Houle, C., Steigmeier, P., Burtscher, H., 2011. Design, Calibration, and Field Performance of a Miniature Diffusion Size Classifier. Aerosol Sci. Technol. 45, 1–10. https://doi.org/10.1080/02786826.2010.516283

Goosse, H., Kay, J.E., Armour, K.C., Bodas-Salcedo, A., Chepfer, H., Docquier, D., Jonko, A., Kushner, P.J., Lecomte, O., Massonnet, F., Park, H.S., Pithan, F., Svensson, G., Vancoppenolle, M., 2018. Quantifying climate feedbacks in polar regions. Nat. Commun. 9. https://doi.org/10.1038/s41467-018-04173-0

HANSEN, A.D.A., ROSEN, H., NOVAKOV, T., 1984. The Aethalometer. Sci. Total Environ. 36, 191–196.

Hanssen-Bauer, I., Førland, E., 2001. Verification and analysis of a climate simulation of temperature and pressure fields over Norway and Svalbard. Clim. Res. 16, 225–235. https://doi.org/10.3354/cr016225

Jacob, D.J., Crawford, J.H., Maring, H., Clarke, A.D., Dibb, J.E., Emmons, L.K., Ferrare, R.A., Hostetler, C.A., Russell, P.B., Singh, H.B., Thompson, A.M., Shaw, G.E., McCauley, E., Pederson, J.R., Fisher, J.A., 2010. The arctic research of the composition of the troposphere from aircraft and satellites (ARCTAS) mission: Design, execution, and first results. Atmos. Chem. Phys. 10, 5191–5212. https://doi.org/10.5194/acp-10-5191-2010

Law, K.S., Roiger, A., Thomas, J.L., Marelle, L., Raut, J.C., Dalsøren, S., Fuglestvedt, J., Tuccella, P., Weinzierl, B., Schlager, H., 2017. Local Arctic air pollution: Sources and impacts. Ambio 46, 453–463. https://doi.org/10.1007/s13280-017-0962-2

Law, K.S., Stohl, A., 2007. Arctic air pollution: Origins and impacts. Science (80-.). 315, 1537–1540. https://doi.org/10.1126/science.1137695

Markowicz, K.M., Ritter, C., Lisok, J., Makuch, P., Stachlewska, I.S., Cappelletti, D., Mazzola, M., Chilinski, M.T., 2017. Vertical variability of aerosol single-scattering albedo and equivalent black carbon concentration based on in-situ and remote sensing techniques during the iAREA campaigns in Ny-Ålesund. Atmos. Environ. 164. https://doi.org/10.1016/j.atmosenv.2017.06.014

Mayer, S., Jonassen, M.O., Sandvik, A., Reuder, J., 2012. Profiling the Arctic Stable Boundary Layer in Advent Valley, Svalbard: Measurements and Simulations. Boundary-Layer Meteorol. 143, 507–526. https://doi.org/10.1007/s10546-012-9709-6

Mayfield, J.A., Fochesatto, G.J., 2013. The layered structure of the winter atmospheric boundary layer in the interior of Alaska. J. Appl. Meteorol. Climatol. 52, 953–973. https://doi.org/10.1175/JAMC-D-12-01.1

Miyakawa, T., Mordovskoi, P., Kanaya, Y., 2020. Evaluation of black carbon mass concentrations using a miniaturized aethalometer: Intercomparison with a continuous soot monitoring system (COSMOS) and a single-particle soot photometer (SP2). Aerosol

Sci. Technol. 54, 811–825. https://doi.org/10.1080/02786826.2020.1724870

Moroni, B., Becagli, S., Bolzacchini, E., Busetto, M., Cappelletti, D., Crocchianti, S., Ferrero, L., Frosini, D., Lanconelli, C., Lupi, A., Maturilli, M., Mazzola, M., Perrone, M.G., Sangiorgi, G., Traversi, R., Udisti, R., Viola, A., Vitale, V., 2015. Vertical Profiles and Chemical Properties of Aerosol Particles upon Ny-Ålesund (Svalbard Islands). Adv. Meteorol. 2015. https://doi.org/10.1155/2015/292081

Moroni, B., Cappelletti, D., Ferrero, L., Crocchianti, S., Busetto, M., Mazzola, M., Becagli, S., Traversi, R., Udisti, R., 2016. Local vs. long-range sources of aerosol particles upon Ny-Ålesund (Svalbard Islands): mineral chemistry and geochemical records. Rend. Lincei 27. https://doi.org/10.1007/s12210-016-0533-7

Roiger, A., Thomas, J.L., Schlager, H., Law, K.S., Kim, J., Schäfler, A., Weinzierl, B., Dahlkötter, F., Risch, I.K., Marelle, L., Minikin, A., Raut, J.C., Reiter, A., Rose, M., Scheibe, M., Stock, P., Baumann, R., Bouarar, I., Lerbaux, C.C., George, M., Onishi, T., Flemming, A.J., 2015. Quantifying emerging local anthropogenic emissions in the arctic region: The access aircraft campaign experiment. Bull. Am. Meteorol. Soc. 96, 441–460. https://doi.org/10.1175/BAMS-D-13-00169.1

Rousseeuw, P.J., Hubert, M., 2011. Robust statistics for outlier detection. WIREs Data Min. Knowl. Discov. 1, 73–79. https://doi.org/10.1002/widm.2

Samset, B.H., Myhre, G., Herber, A., Kondo, Y., Li, S.M., Moteki, N., Koike, M., Oshima, N., Schwarz, J.P., Balkanski, Y., Bauer, S.E., Bellouin, N., Berntsen, T.K., Bian, H., Chin, M., Diehl, T., Easter, R.C., Ghan, S.J., Iversen, T., Kirkevåg, A., Lamarque, J.F., Lin, G., Liu, X., Penner, J.E., Schulz, M., Seland, Skeie, R.B., Stier, P., Takemura, T., Tsigaridis, K., Zhang, K., 2014. Modelled black carbon radiative forcing and atmospheric lifetime in AeroCom Phase II constrained by aircraft observations. Atmos. Chem. Phys. 14, 12465–12477. https://doi.org/10.5194/acp-14-12465-2014

Schmale, J., Arnold, S.R., Law, K.S., Thorp, T., Anenberg, S., Simpson, W.R., Mao, J., Pratt, K.A., 2018. Local Arctic Air Pollution: A Neglected but Serious Problem. Earth's Futur. 6, 1385–1412. https://doi.org/10.1029/2018EF000952

Schulz, H., Zanatta, M., Bozem, H., Richard Leaitch, W., Herber, A.B., Burkart, J., Willis, M.D., Kunkel, D., Hoor, P.M., Abbatt, J.P.D., Gerdes, R., 2019. High Arctic aircraft measurements characterising black carbon vertical variability in spring and summer. Atmos. Chem. Phys. 19, 2361–2384. https://doi.org/10.5194/acp-19-2361-2019

Serreze, M.C., Barry, R.G., 2011. Processes and impacts of Arctic amplification: A research synthesis. Glob. Planet. Change 77, 85–96. https://doi.org/10.1016/j.gloplacha.2011.03.004

Shibata, T., Shiraishi, K., Shiobara, M., Iwasaki, S., Takano, T., 2018. Seasonal Variations in High Arctic Free Tropospheric Aerosols Over Ny-Ålesund, Svalbard, Observed by Ground-Based Lidar. J. Geophys. Res. Atmos. 123, 12,353-12,367. https://doi.org/10.1029/2018JD028973

Stein, A.F., Draxler, R.R., Rolph, G.D., Stunder, B.J.B., Cohen, M.D., Ngan, F., 2015. Noaa's hysplit atmospheric transport and dispersion modeling system. Bull. Am. Meteorol. Soc. 96, 2059–2077. https://doi.org/10.1175/BAMS-D-14-00110.1

Su, T., Li, Z., Li, C., Li, J., Han, W., Shen, C., Tan, W., Wei, J., Guo, J., 2020. The significant impact of aerosol vertical structure on lower atmosphere stability and its critical role in aerosol-planetary boundary layer (PBL) interactions. Atmos. Chem. Phys. 20, 3713–3724. https://doi.org/10.5194/acp-20-3713-2020

Thomas, M.A., Devasthale, A., Tjernström, M., Ekman, A.M.L., 2019. The Relation Between Aerosol Vertical Distribution and Temperature Inversions in the Arctic in Winter and Spring. Geophys. Res. Lett. 46, 2836–2845. https://doi.org/10.1029/2018GL081624

Wallace, J.M., Hobbs, P. V., 2006. Atmospheric science: an introductory survey, 2nd ed.

Academic Press, New York.

Wang, X.Y., Wang, K.C., 2014. Estimation of atmospheric mixing layer height from radiosonde data. Atmos. Meas. Tech. 7, 1701–1709. https://doi.org/10.5194/amt-7-1701-2014

TABLES

Table 1 - Characteristics of 50m averaged *eBC*and *NP* profiles recorder in Adventdalen. Median concentrations are compared with median values of maximum concentrations (MMC) and MMC height and *eBC* concentration in Longyearbyen (LYB, from AE33). These are calculated for the period of two hours before the sounding to the time of tethered balloon launch with eBC sensor in Adventdalen. *zTb* is the height of the temperature inversion.

Group profiles	Number		Median concentration		MMC		MMC height		LYB Median
	eBC	*NP*	*eBC*, $ng \cdot m^{-3}$	*NP*, cm^{-3}	*eBC*, $ng \cdot m^{-3}$	*NP*, cm^{-3}	*eBC* *m*	*NP* *m*	*eBC*, $ng \cdot m^{-3}$
No temp inversion	43	32	94	**483**	**147**	**644**	350	**100**	**158**
zTb<500m	25	16	94	**1745**	**210**	**3080**	100	**0**	**181**
zTb>=500m	6	0	110	-	**194**	-	550	-	**199**

FIGURES

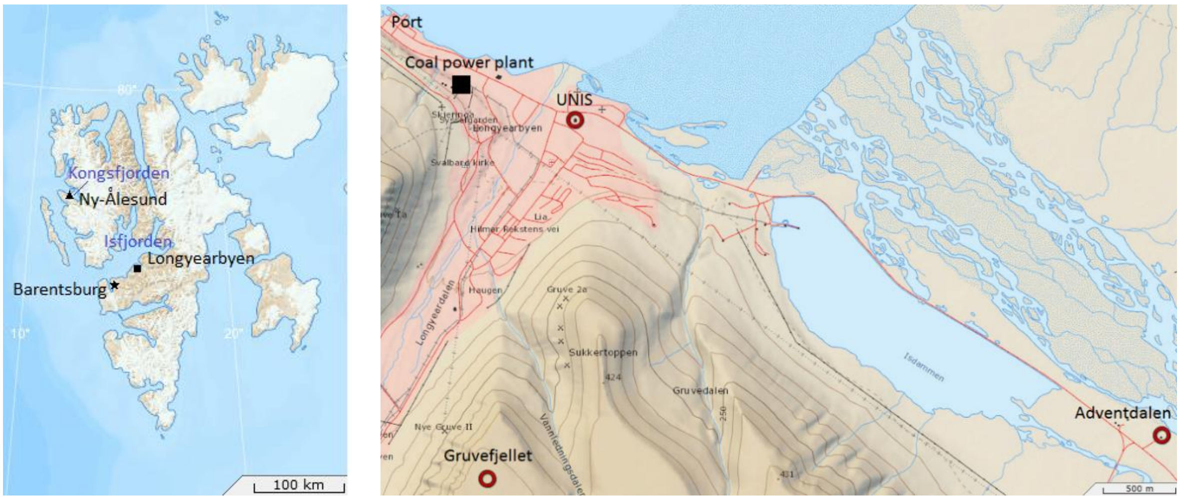

Figure 1. Left) Map of Svalbard; right) local map of Longyearbyen (the launching site is marked with the red circle in the Adventdalen valley)

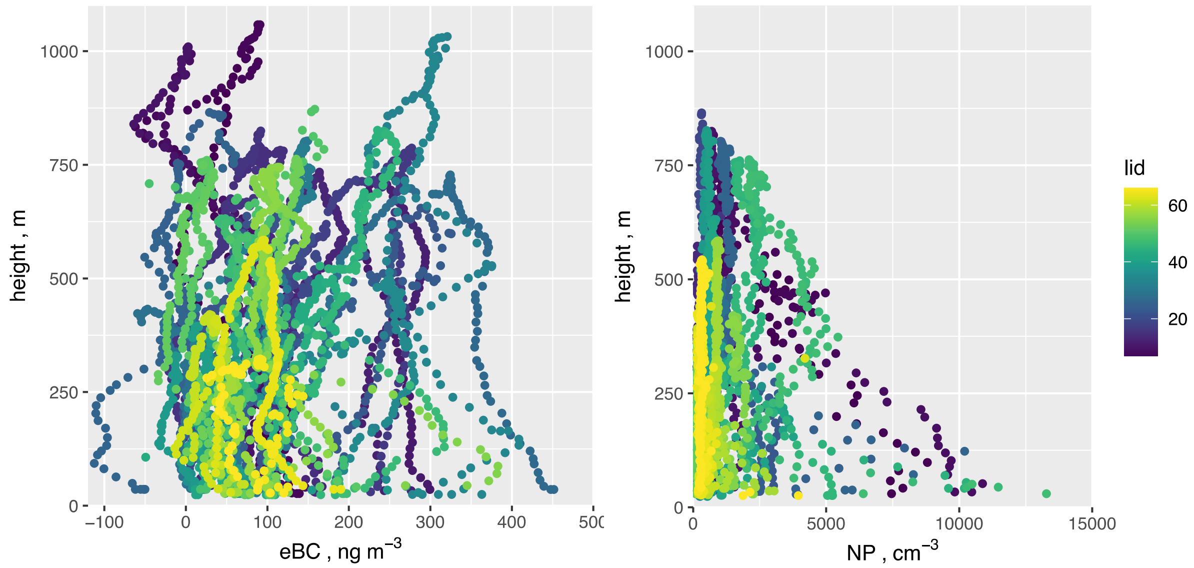

Figure 2 – Ungridded vertical profiles of (a) *eBC* and (b) *NP*. The colour scale identifies the launch identification (lid).

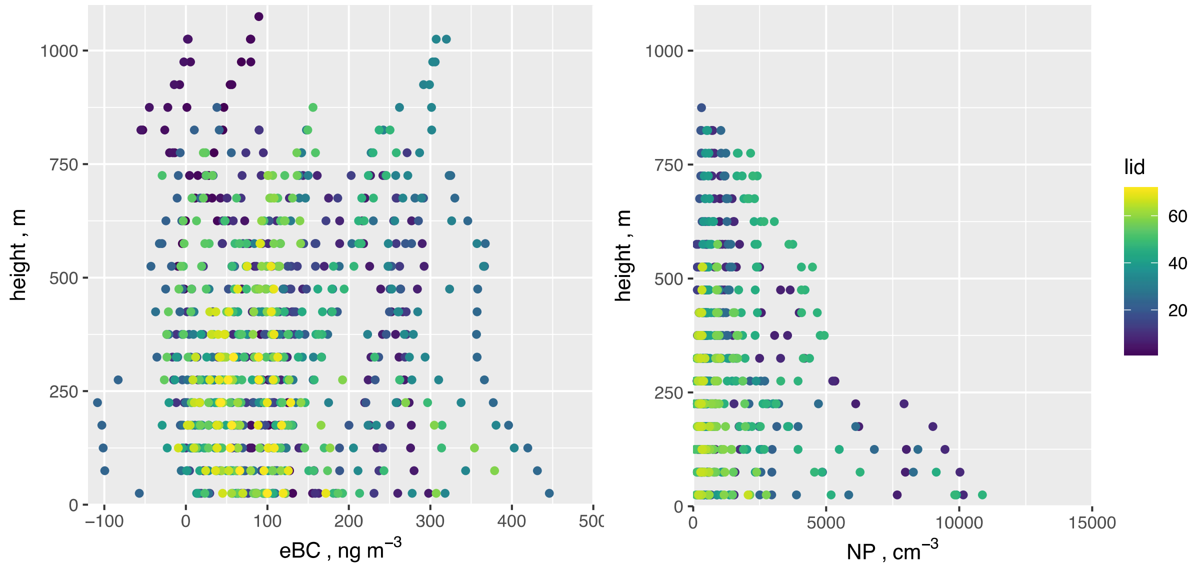

Figure 3 – Gridded vertical profiles of (a) *eBC*and (b) *NP*. The colour scale identifies the launch identification (lid).

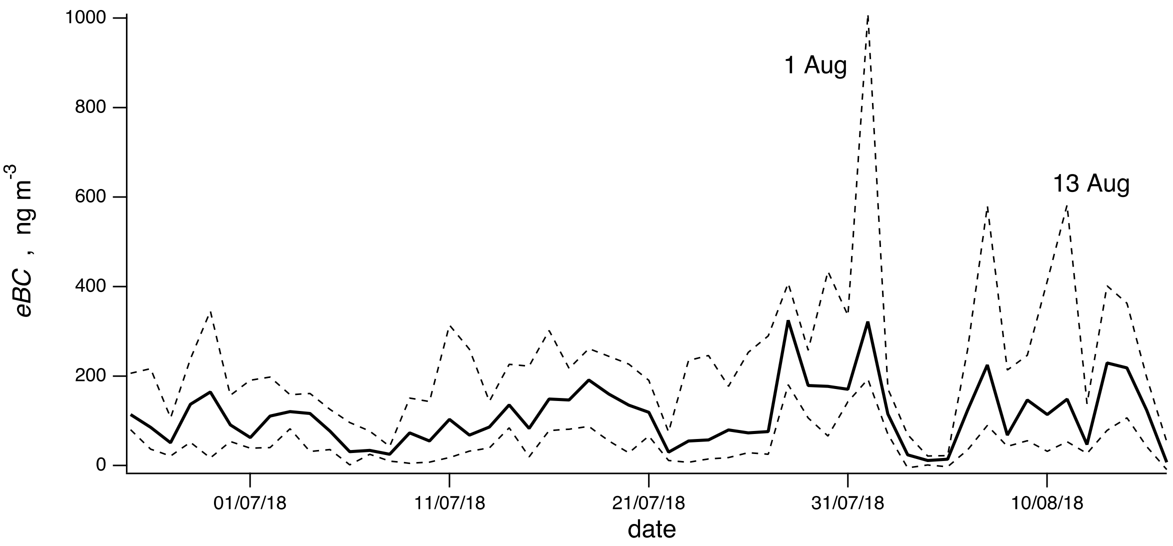

Figure 4 – Daily median *eBC* values measured in LYB with the AE33. Dashed lines indicate the 25 and 75 percentiles.

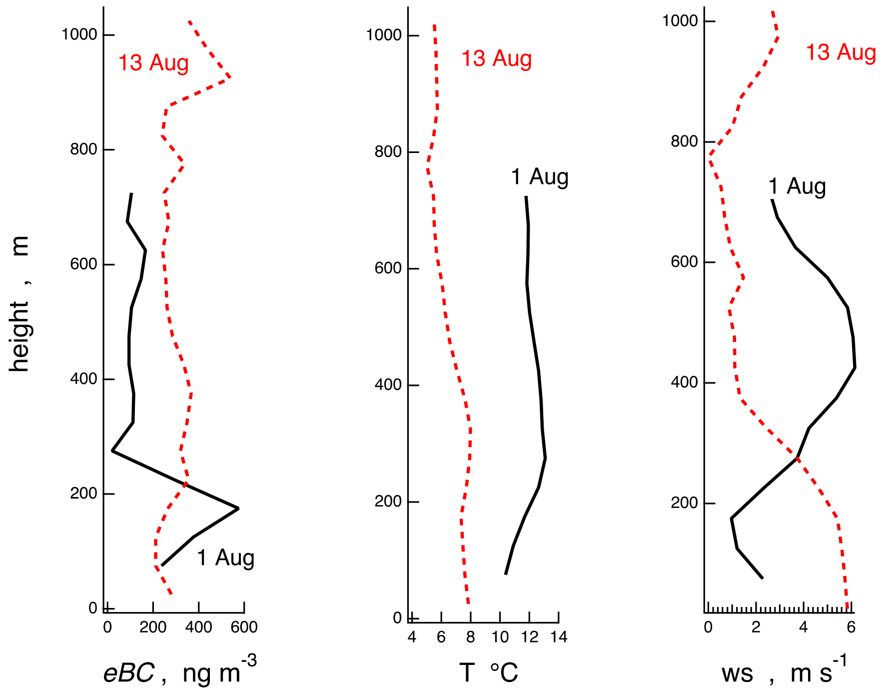

Figure 5 – Vertical profiles of eBC, temperature and wind speed registered with the tethered balloon system on the 1st of August (black continuous lines) and on the 13 of August (red dashed lines).

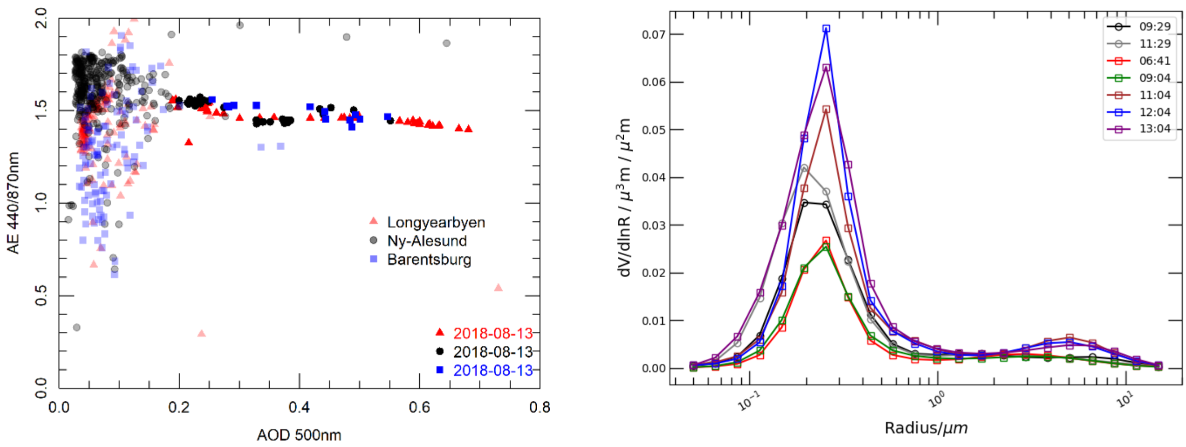

Figure 6 – Lefthand panel: Angstrom Exponent 440/870 nm as a function of the AOD at 500 nm; righthand panel: size distribution inversions for August 13th for Longyearbyen and Ny-Ålesund.

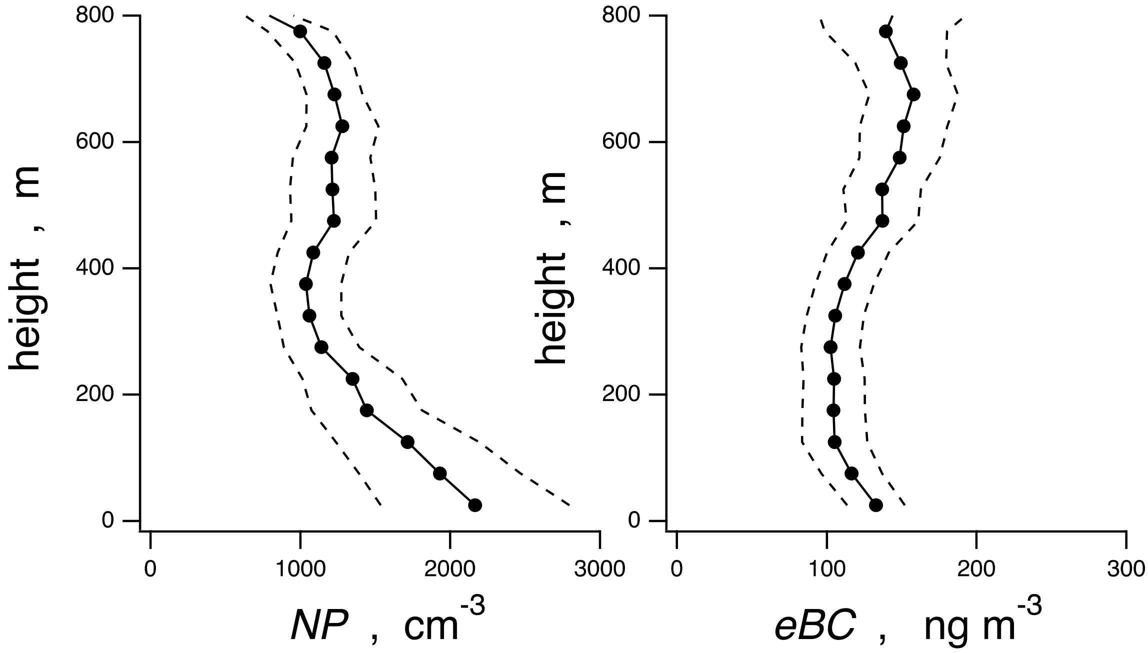

Figure 7 – Summertime averaged *eBC* (a) and *NP* (b) profiles along the atmospheric column over Longyearbyen in 2018. Dashed lines represent the 95% confidence interval of the population.

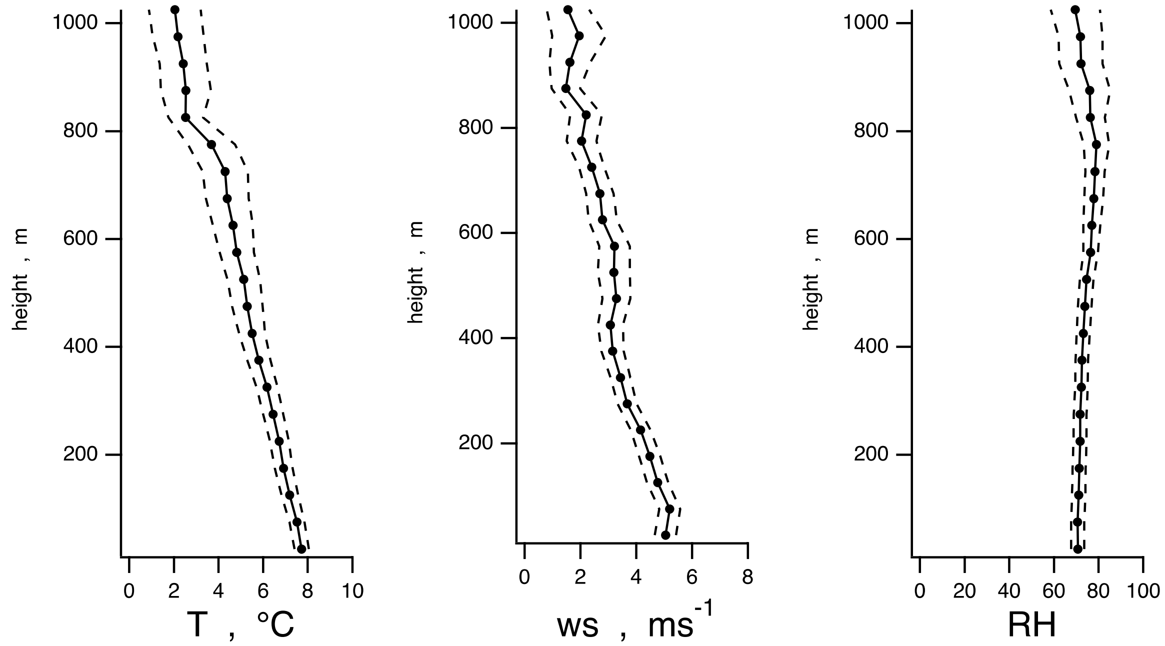

Figure 8 – Summertime averaged *T* (a), *RH* (b) and wind speed (*ws*)(c) profiles along the atmospheric column over Longyearbyen in 2018. Dashed lines represent the 95% confidence interval of the population.